Original Article

Institution of MECHANICAL ENGINEERS

Journal of SYSTEMS AND CONTROL ENGINEERING

Proc IMechE Part I:
J Systems and Control Engineering
1–10

DOI: 10.1177/0959651816656749
pii.sagepub.com
SAGE

Cascade sliding mode–based robust tracking control of a magnetic levitation system

Yakup Eroğlu and Günyaz Ablay

Abstract

Magnetic levitation systems are able to provide frictionless, reliable, fast and economical operations in wide-range applications. The effectiveness and applicability of these systems require precise feedback control designs because the magnetic levitation is an unstable process and have highly nonlinear dynamics. In this article, a robust sliding mode–based cascade control approach is proposed for effectively tracking the reference position of a magnetic levitation system. The magnetic levitation plant is described with electrical and mechanical models, and the control problems of these parts are treated with cascade controllers. An integral sliding mode and an output feedback sliding mode controllers are designed for use in the cascade loops. The performance of the sliding mode controllers is compared with a proportional–integral–velocity plus proportional–integral control structure. It is shown that the proposed control structure is able to provide a highly satisfactory tracking performance and can eliminate the effects of the inductance-related uncertainties and operating point originated disturbances. The experimental results are provided to validate the efficacy and feasibility of the approach.

Keywords

Magnetic levitation, maglev, sliding mode control, cascade control, robust tracking

Date received: 19 March 2016; accepted: 31 May 2016

Introduction

Magnetic levitation technology provides contactless movement and removes friction problem. It has been used in many industrial systems including high-speed maglev trains, frictionless bearings, electromagnetic cranes, levitation of wind tunnel models, vibration isolation of sensitive machinery, levitation of molten metal in induction furnaces, rocket-guiding projects, levitation of metal slabs during manufacture and high-precision positioning of wafers in photolithography.[1–9] This technology is capable of serving reliable and high-speed operations with the use of feedback controllers. On the other hand, it is difficult to provide a high control performance with standard controllers for the magnetic levitation systems because of their open-loop unstable and highly nonlinear dynamics, and the existence of parameter uncertainties originated by the inductance of the electromagnetic coil.

Recently, many works have been reported for controlling magnetic levitation in the literature. The designed control techniques include feedback linearization-based controllers (including input–output and input-state linearization techniques),[6,7,10–13] linear state feedback control design,[7,14] the gain scheduling approach,[15] observer-based control,[4,16] cognitive techniques,[17–19] sliding mode controllers,[9,20,21] backstepping control,[22] model predictive control,[23,24] adaptive and H-inf controllers[25] and proportional–integral–derivative (PID) controllers.[16,26] In short, many known linear and nonlinear control methods were designed for magnetic levitation systems. In the linear controller designs, the approximate linear model found by perturbing the system dynamics about a desired operating point is used, and thus, the controllers are usually valid around the operating point. The performance of the linear controllers can be improved with some kind of gain scheduling procedure to change operating points,

Department of Electrical-Electronics Engineering, Abdullah Gül University, Kayseri, Turkey

Corresponding author:
Günyaz Ablay, Department of Electrical-Electronics Engineering, Abdullah Gül University, Kayseri 38080, Turkey.
Email: gunyaz.ablay@agu.edu.tr

but the stability may not be guaranteed. Since the governing differential equations are highly nonlinear, the nonlinear controllers seem more attractive. However, many nonlinear control designs need exact knowledge about the plant nonlinearities to ensure a good performance. The modeling and parameter uncertainties in the magnetic levitation plant model make practical implementations of the nonlinear controllers difficult.

In this work, a practical cascade control approach constructed with robust sliding mode controllers is proposed for controlling a magnetic levitation plant. The cascade control allows us to design a fast and high-gain inner loop current controller to deal with the effects of plant disturbance and uncertainties. The sliding mode control (SMC) methodology has the ability to render robustness in the presence of parameter uncertainties and operating point variations An integral SMC is designed for the outer loop (mechanical part) of the system and an output feedback SMC is proposed for the inner loop (electrical part) control. The effectiveness of the method is compared with a proportional–integral–velocity (PIV) plus PI controller and demonstrated with experimental tests. It is shown that the SMC plus SMC-based cascade controller can provide highly satisfactory tracking performance with a small tracking error for the magnetic levitation system in the existence of uncertainties.

This article is organized as follows: section "Magnetic levitation and modeling" describes the possible models of the maglev system. Section "Controller design" presents our proposed robust control scheme and a traditional PIV plus PI control structure in detail. The experimental results are illustrated in section "Experimental results." Finally, the concluding remarks are provided in section "Conclusion."

Magnetic levitation and modeling

The magnetic levitation system is used to levitate a ferromagnetic object in air through the electromagnetic force generated by an electromagnet. The system we work on is composed of an electromagnet, a steel ball, a position measurement sensor, a data acquisition board, a power source and a computer. The photograph of the experimental setup of the magnetic levitation system for single-axis control is shown in Figure 1.

The magnetic levitation plant (Quanser model) is composed of an electromagnet, a steel ball, a ball post and a ball position sensor. The ball can only be controlled through vertical x-axis. The attraction force is controlled by the computer-controlled electromagnet mounted directly above the levitation ball. The photo detector consists of an NPN silicon photodarlington. The electromagnet is composed of a tightly wound solenoid coil made of 2450 turns of 20 AWG magnet wire. Electromagnet coil input supply is ± 24 V with a maximum of 3 A coil current. The data acquisition board is a successive approximation type, 12-bit analog and digital conversion board capable of 4 kHz sampling. In this work, the controllers are implemented at a sampling rate of 1 kHz. The other plant parameters used in experimental studies are summarized in Table 1.

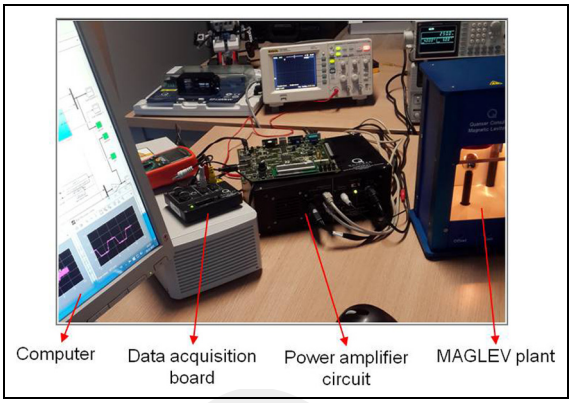

Figure 1. Experimental setup of a single-axis magnetic levitation system.

Table 1. Magnetic levitation plant parameters.

Symbol	Description	Value
L	Coil inductance	412.5 mH
R	Coil resistance	10 Ω
R_s	Current sense resistance	1 Ω
k	Electromagnet force constant	6.53×10^{-5} N m^2/A^2
m	Steel ball mass	0.068 kg
K_B	Position sensor sensitivity	2.83×10^{-3} m/V
N_c	Number of turns in coil wire	2450
μ_0	Magnetic permeability constant	$4\pi \times 10^{-7}$ H/m

To use in analysis and control design, the model of the magnetic levitation system can obtained by applying the first principle–based approach to the mechanical and electrical parts of the system as seen in Figure 2. The electromagnet is modeled with the RL network while the mechanical part is expressed in terms of acting forces. The ball position of the mechanical part of the system is controlled via the coil current, I, whereas the coil current of the electrical part of the system is regulated with the applied voltage. Therefore, the voltage applied to the electromagnet indirectly controls the ball position. In the following sections, we describe and analyze the mathematical models of the system.

Modeling of the mechanical part

Using the notation and conventions given in Figure 2, the mechanical model of the plant can be obtained. By applying Newton's second law of motion to the ball, the force balance equation of the ball is given with the following second-order model

$$m\ddot{x} = mg - f(x, I) \tag{1}$$

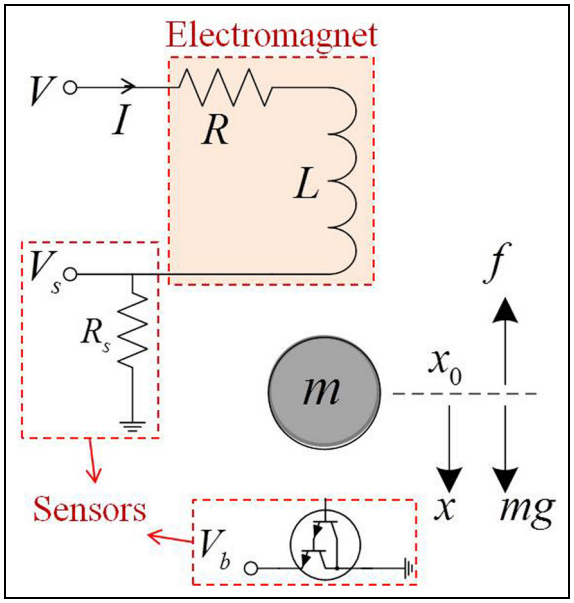

Figure 2. First principle–based dynamical modeling of the magnetic levitation system.

where x is the air gap (in m), m is the mass of the ball (in kg), g is the gravitational constant (in m/s^2) and $f(\cdot)$ is the force generated by the electromagnet (in N). The attractive force generated by the electromagnet is given by[27]

$$f(x, I) = -\frac{I^2}{2}\frac{dL}{dx} \tag{2}$$

The inductance L has its largest value when the ball is next to the coil, but decreases to a constant L_1 as x goes to infinity. While several approximations can be used to express the inductance,[7,16] it can be assumed that

$$L(x) = L_1 + \frac{L_0 x_0}{x} = L_1 + \frac{k}{x} \tag{3}$$

where L_0 is a constant around the operating point x_0. Obviously, this assumption causes parameter uncertainty in the plant model, but results in a simplified model. Substituting equation (3) into equation (2), one can obtain

$$f(x, I) = \frac{k}{2}\left(\frac{I}{x}\right)^2 \tag{4}$$

where k is the electromagnetic force constant (in N m^2/A^2) and I is the coil current (in A). Now, the operating point (or equilibrium point) of the system can be specified when all the time-derivative terms in equation (1) are set to 0, $\dot{x} = \ddot{x} = 0$

$$I_0 = x_0\sqrt{2\,\mathrm{mg/k}} \tag{5}$$

where the operating point of the coil current, I_0, is expressed as a function of operating position x_0. This operating point (x_0, I_0) will be used to analyze the system and to determine control gains.

In order to simplify analysis of the magnetic levitation plant, the system can be linearized around the equilibrium point (x_0, I_0). By applying the Taylor series approximation about equilibrium point (x_0, I_0), model (1) can be written as

$$\ddot{x} = g - \frac{kI_0^2}{2mx_0^2} + \frac{kI_0^2}{mx_0^3}x - \frac{kI_0}{mx_0^2}I \tag{6}$$

Substituting equation (5) into equation (6), we get a linear model for the mechanical part of the system as

$$\ddot{x} = \frac{2g}{x_0}x - \frac{2g}{I_0}I \tag{7}$$

The transfer function of equation (7) is then

$$G_b(s) = \frac{X(s)}{I(s)} = -\frac{K_b w_b^2}{s^2 - w_b^2} \tag{8}$$

where $K_b = (x_0/I_0)$ and $w_b = \sqrt{2g/x_0}$. The open-loop transfer function model (8) of the magnetic levitation system indicates that the open-loop system is unstable since the poles are located at $s_{1,2} = \pm w_b$. Hence, a feedback controller is needed to stabilize the system and to provide a good tracking performance.

Modeling of the electrical part

The electrical model of the system can be expressed in two ways, that is, one is a linear model for the constant coil inductance assumption and the other one is a nonlinear model for the time-varying inductance. By applying Kirchhoff's voltage law to the electromagnet modeled by the RL network as seen in Figure 2, we can get the model of the electrical part directly as

$$\frac{dI}{dt} = -\frac{R + R_s}{L}I + \frac{1}{L}V \tag{9}$$

where I is the coil current (in A), L is the coil inductance (in H), R is the coil resistance (in Ω), R_s is the current sense resistance (in Ω) and V is the supply voltage (in V). The transfer function of the linear model is

$$G_e(s) = \frac{I(s)}{V(s)} = \frac{K_e}{\tau_e s + 1} \tag{10}$$

where $K_e = 1/(R + R_s)$ is the DC gain, and $\tau_e = L/(R + R_s)$ is the time constant of the electrical subsystem. On the other hand, when the time-varying inductance is taken into account, the electrical model takes the following nonlinear form

$$\frac{dI}{dt} = -\frac{R + R_s}{L}I + \frac{k}{L}\frac{\dot{x}}{x^2}I + \frac{1}{L}V \tag{11}$$

The nonlinear model (11) implies that the ball cannot contact with the electromagnet during operations, that is, $x \neq 0$. Since the coil inductance value is dependent on the ball position, x, and we assume that it is a

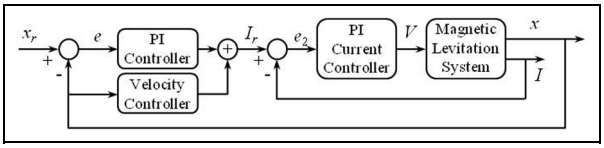

Figure 3. PIV plus PI cascade control scheme of the magnetic levitation system.

constant around the operation point (x_0/I_0), there exists a parameter uncertainty on the coil inductance of the model. Thus, we need to design a robust controller to eliminate the effects of the parameter uncertainty.

Controller design

Since the inner electrical part of the system is much faster than the outer mechanical part due to their natural behaviors, a cascade control structure can perform better than a traditional control structure. It is also possible to design advanced control methods in the cascaded loops to acquire superior performances. Therefore, this work focuses on a cascade control of the magnetic levitation system for achieving stability, robustness and a highly satisfactory position tracking performance. In the following sections, a cascaded SMC controller will be proposed and its performance will be compared with a traditional PIV plus PI controller.

Design of a PIV plus PI cascade controller

The PIV plus PI-based cascade controller for the magnetic levitation system is illustrated in Figure 3. The PIV controller is designed for controlling the outer position loop, while the PI controller is considered for controlling the inner current loop.

First, let us design a PI controller for the inner current loop as

$$V(t) = k_{pe}(I_r(t) - I(t)) + k_{ie}\int (I_r(t) - I(t))dt \tag{12}$$

If we take Laplace transform of equation (12) and substitute it into the electrical model (10), the closed-loop transfer function for the electrical part turns out to be

$$\frac{I(s)}{I_r(s)} = \frac{K_e k_{pe} s + K_e k_{ie})}{\tau_e s^2 + (K_e k_{pe} + 1)s + K_e k_{ie}} \tag{13}$$

Now, assume that the desired performance requirements of the inner current loop are described by a damping ratio ς_e and a natural frequency of w_{ne}. To achieve these desired performance requirements, since the transfer function of the inner loop is of second-order, the following characteristic equation can be constructed

$$s^2 + 2\zeta_e w_{ne} s + w_{ne}^2 = 0 \tag{14}$$

and using pole placement method, which compares the characteristic equation of closed-loop system (13) with the desired characteristic equation (14), the appropriate PI control gains, k_{pe} and k_{ie}, for the inner current loop can be calculated as

$$k_{pe} = \frac{2\zeta_e w_{ne}\tau_e - 1}{K_e}, k_{ie} = \frac{w_{ne}^2 \tau_e}{K_e} \tag{15}$$

Second, a PIV controller with set point weighting for controlling the outer mechanical part can be designed by

$$I_r(t) = k_{pb}\left(b_{sp}x_r(t) - x(t)\right) + k_{ib} \int (x_r(t) - x(t))dt - k_{vb}\dot{x}(t) \tag{16}$$

To use this controller, we can first obtain the closed-loop transfer function of the mechanical part as

$$\frac{X(s)}{X_r(s)} = \frac{I_r(s)}{X_r(s)}\frac{V(s)}{I_r(s)}\frac{I(s)}{V(s)}\frac{X(s)}{I(s)} = \frac{I_r(s)}{X_r(s)}\frac{V(s)}{I_r(s)}\frac{I(s)}{V(s)}G_b(s) \tag{17}$$

Here, it is assumed that $I_r(s) = I(s)$ due to the fast inner control loop, and thus, we have

$$\frac{V(s)}{I_r(s)}\frac{I(s)}{V(s)} = 1 \tag{18}$$

For this reason, the closed-loop transfer function of the mechanical part becomes

$$\frac{X(s)}{X_r(s)} = \frac{I_r(s)}{X_r(s)}G_b(s) \tag{19}$$

Substituting the transfer function of the PIV controller (16) into equation (19), we get

$$\frac{X(s)}{X_r(s)} = \frac{2gx_0(k_{pb}b_{sp}s + k_{ib})}{-I_0x_0s^3 + 2gx_0k_{vb}s^2 + 2g(x_0k_{pb} + I_0)s + 2gx_0k_{ib}} \tag{20}$$

To calculate the gains of the PIV controller, if we assume that the desired performance requirements of the system are given by a damping ratio ς_b and a natural frequency of w_{nb}, then since the transfer function (20) is of third-order, a desired characteristic equation can be constructed from the desired requirements as

$$(s^2 + 2\zeta_b w_{nb}s + w_{nb}^2)(s + p_0) = 0 \tag{21}$$

Then, by comparing the characteristic equation of system (20) with the desired characteristic equation (21), the control gains of the PIV controller are found as

$$k_{pb} = -\frac{(2p_0\zeta_b w_{nb}x_0 + w_{nb}^2x_0 + 2g)I_0}{2x_0}, k_{ib} = -\frac{p_0w_{nb}^2I_0}{2g}$$
$$k_{vb} = -\frac{(p_0 + 2\zeta_b w_{nb})I_0}{2g}, b_{sp} = 1 + \frac{I_0}{k_{pb}x_0} \tag{22}$$

Here, there are three significant points that we have to clarify. First, the third pole (p_0) must be two to five times farther than the dominant pole to obtain a good

feedback response. Second, set point weighting, b_{sp}, is used to eliminate the changes in the force created due to gravitational bias. Hence, the set point weighting is applied to the proportional controller to have a good steady-state response. Third, due to the noise in the measurements, a second-order derivative filter is designed to filter out noise when acquiring the velocity state from the position measurement as

$$G_d(s) = \frac{w_d^2 s}{s^2 + 2\zeta_d w_d s + w_d^2} \tag{23}$$

By considering the derivative filter (23), the characteristic equation of the closed-loop system can be obtained as

$$\begin{aligned} &s^5 + 2\zeta_d w_d s^4 + (w_d^2 - w_b^2 - K_b k_{pb} w_b^2)s^3 \\ &- (2\zeta_d w_d w_b^2 + 2\zeta_d w_d K_b k_{pb} w_b^2 + K_b k_{ib} w_b^2 + K_b k_{vb} w_d^2 w_b^2)s^2 \\ &- (w_d^2 w_b^2 + K_b k_{pb} w_d^2 w_b^2 + 2\zeta_d w_d w_b^2 K_b k_{ib})s - (K_b k_{ib} w_d^2 w_b^2) = 0 \end{aligned} \tag{24}$$

where the filter parameters ς_d and w_d should be selected appropriately using the known control parameters given in equation (22). It is clear that the stability of equation (24) is ensured if the roots of the derivative filter (24) are selected as two to five times farther than the dominant pole of the closed-loop system (21). However, to achieve the desired system dynamics the roots of equation (24) should be selected as 30 times farther than the closed-loop dominant poles.

Design of an SMC plus SMC cascade controller

SMC methodology is well-known with its robustness against system uncertainties and with its high control performance through suitable designs. In this section, an SMC plus SMC cascade controller is designed for controlling the magnetic levitation plant. The proposed control structure is illustrated in Figure 4. It is very unusual to design SMC methods in cascade forms, but we will show that it is possible to get a highly satisfactory control performance with cascade SMCs.

An integral SMC for the outer mechanical part. The integral sliding mode controller is designed for the outer loop to control the ball position of the magnetic levitation system. Here, similar to equation (18), first we assume that $I_r = 1$ to decrease the complexity of the designs. Thus, we focus on the mechanical part of the system to control the ball position. To design an integral sliding mode controller, an integral sliding surface s_1 is first defined for the second-order mechanical model of system as

$$s_1 = \dot{e} + \lambda e + \lambda_0 \int e dt \tag{25}$$

where $e = x_r - x$ and $\lambda, \lambda_0 = 0$. The integral action is designed to ensure accurate position tracking. In order to design an appropriate controller, the time-derivative of the sliding surface (25) is written as below with the mechanical dynamics (8)

$$\dot{s}_1 = \ddot{x}_r - w_b^2 x + K_b w_b^2 I + \lambda(\dot{x}_r - \dot{x}) + \lambda_0(x_r - x) \tag{26}$$

If a sliding mode exists, then during the sliding mode, that is, $s_1 = \dot{s}_1 = 0$, the equivalent current term, I_{eq}, can be obtained as follows

$$I_{eq} = -\frac{1}{K_b w_b^2}\left[\ddot{x}_r - w_b^2 x + \lambda(\dot{x}_r - \dot{x}) + \lambda_0(x_r - x)\right] \tag{27}$$

Now, the SMC law can be written as

$$I = I_{eq} - I_m \,\mathrm{sat}\left(\frac{s_1}{\varepsilon}\right) \tag{28}$$

where

$$\mathrm{sat}(s) = \begin{cases} \mathrm{sgn}(s/\varepsilon), & \text{if} \quad |s| \geqslant \varepsilon \\ s/\varepsilon, & \text{if} \quad |s| < \varepsilon \end{cases} \tag{29}$$

where $\varepsilon > 0$ and the $\mathrm{sgn}(\cdot)$ is the signum function. The saturation function, $\mathrm{sat}(\cdot)$, is used to eliminate chattering on the system output. Note that a second-order sliding mode algorithm (e.g. super-twisting algorithm) can also be considered to reduce chattering, but a complete chattering elimination is not possible with second-order SMCs under modeling errors and measurement noise.[28] The equivalent current controller is used in the control structure because it is necessary to keep the system trajectory on the sliding surface and to help eliminating possible chattering phenomenon.

The stability of the system under the integral SMC must be achieved. First, if a positive definite Lyapunov function is defined by

$$V_1 = \frac{{s_1}^2}{2} \tag{30}$$

then its derivative must be negative definite for stability, that is

$$\begin{aligned} \dot{V}_1 &= s_1 \dot{s}_1 \\ &= s_1\left(\ddot{x}_r - w_b^2 x + K_b w_b^2 I + \lambda(\dot{x}_r - \dot{x}) + \lambda_0(x_r - x)\right) \\ &= s_1\left(-K_b w_b^2 I_m \,\mathrm{sat}(s_1)\right) \end{aligned} \tag{31}$$

It is clear from equation (29) that the controller consists of the outer and inner parts. For the outer part of the controller, that is, for $|s_1| \geqslant \varepsilon$, we have

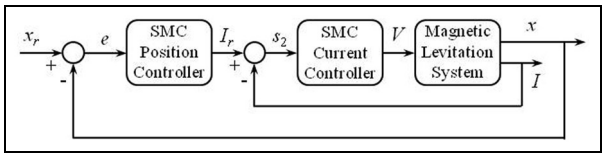

Figure 4. SMC plus SMC cascade control scheme for the magnetic levitation system.

$$\begin{aligned}\dot{V}_1 &= -K_b w_b^2 I_m s_1 \operatorname{sgn}(s_1/\varepsilon)\\ &= -K_b w_b^2 I_m \frac{s_1/\varepsilon}{|s_1/\varepsilon|} s_1\\ &= -K_b w_b^2 I_m |s_1|\end{aligned} \tag{32}$$

Since K_b and w_b are positive, if we choose $I_m > 0$, then $\dot{V}_1 < 0$. That is to say, whenever $|s_1| \geq \varepsilon$, $|s_1(t)|$ will strictly decrease until it reaches the set $|s_1| < \varepsilon$ in finite time and remains inside the set subsequently. For the inner part of the controller, that is, inside the set $|s_1| < \varepsilon$, the derivative of the Lyapunov function can similarly be written as

$$\dot{V}_1 = -K_b w_b^2 I_m s_1^2/\varepsilon \tag{33}$$

Again if $I_m > 0$, then $\dot{V}_1 < 0$. Consequently, the practical stability of the outer part with the proposed integral SMC controller is guaranteed whenever the control gain $I_m > 0$.

Robustness of the integral sliding mode position controller. If we assume that there is an uncertainty in the system dynamics due to the operating point variation and linearization, the dynamics of the mechanical part (8) can be written as

$$\ddot{x} - \left(w_b^2 + d_1(x_0)\right)x + \left(K_b w_b^2 + d_1(x_0)\right)I = 0 \tag{34}$$

where it is assumed that $(K_b w_b^2 + d_1(x_0)) > 0$ and $d_1(x_0)$ represents the system uncertainties. Now, the derivative of the sliding surface (25) can be given by

$$\begin{aligned}\dot{s}_1 = \ddot{x}_r &- (w_b^2 + d_1)x + (K_b w_b^2 + d_1)I\\ &+ \lambda(\dot{x}_r - \dot{x}) + \lambda_0(x_r - x)\end{aligned} \tag{35}$$

For the same Lyapunov function $V_1 = s_1^2/2$, the time-derivative of it is

$$\begin{aligned}\dot{V}_1 &= s_1\left(\ddot{x}_r - (w_b^2 + d_1)x + (K_b w_b^2 + d_1)I\right.\\ &\quad \left. + \lambda(\dot{x}_r - \dot{x}) + \lambda_0(x_r - x)\right)\\ &= s_1\left(-d_1 x - K_b w_b^2 I_m \operatorname{sat}(s_1) + d_1 I_{eq} - d_1 I_m \operatorname{sat}(s_1)\right)\end{aligned} \tag{36}$$

For the outer part of the controller, that is, for $|s_1| \geq \varepsilon$, by applying Cauchy–Schwarz inequality, we have

$$\begin{aligned}\dot{V}_1 &= -d_1 x s_1 + d_1 I_{eq} s_1 - (K_b w_b^2 + d_1) I_m \frac{s_1/\varepsilon}{|s_1/\varepsilon|} s_1\\ &\leq |d_1 x||s_1| + \left|d_1 I_{eq}\right||s_1| - (K_b w_b^2 + d_1) I_m |s_1|\\ &= \left(|d_1 x| + \left|d_1 I_{eq}\right| - (K_b w_b^2 + d_1) I_m\right)|s_1|\end{aligned} \tag{37}$$

Therefore, if we choose $I_m \geq d_1(|x| + |I_{eq}|)/(K_b w_b^2 + d_1)$, then it is guaranteed that the system trajectory will enter the inner boundary layer, $|s_1| < \varepsilon$, and stay there. It should be noted that for the magnetic levitation system under study, since the coil current works in the range of $0 \leq I \leq 3$ A, the extreme values of the uncertainty $d_1(x_0)$ can be

$$d_1 < K_b w_b^2 = 2g/I_0 \Rightarrow d_1 < 6.54 \tag{38}$$

Hence, the stability of the uncertain system under integral SMC is guaranteed for our system as long as the uncertainty satisfies $d_1(x_0) < 6.54$.

An output feedback SMC for the inner electrical part. SMC can also be considered to control the coil current due to its fast response and robustness features. Since the coil inductance is the function of the ball position, there exists a parameter uncertainty. The effects of inductance-related uncertainties can be minimized by designing a high-gain SMC for controlling electrical part of the system current. To design an SMC, first a sliding surface, s_2, is given by

$$s_2 = I_r - I \tag{39}$$

The time-derivative of equation (39) with the nonlinear electrical model (11) is then

$$\dot{s}_2 = \dot{I}_r + \frac{R + R_s}{L} I - \frac{k}{L}\frac{I\dot{x}}{x^2} - \frac{1}{L} V \tag{40}$$

To achieve a sliding mode, that is, $s_2 = \dot{s}_2 = 0$, the voltage V as the control input of the magnetic levitation can be designed as[29]

$$\begin{aligned}V &= \alpha |s_2|^{1/2} \operatorname{sat}(s_2) + u_1\\ \dot{u}_1 &= \beta |s_2|^{1/2} \operatorname{sat}(s_2)\end{aligned} \tag{41}$$

where the sat$(\cdot)$ function is defined in equation (29). The stability of the electrical dynamics under the SMC must be satisfied with appropriate selection of the gains, α and β. For a positive definite Lyapunov function

$$V_2 = \frac{1}{2} s_2^2 + \frac{1}{2} u_1^2 \tag{42}$$

its time-derivative with the electrical model (11), sliding surface (39) and controller (41) can be written as

$$\dot{V}_2 = s_2\left(\dot{I}_r + \frac{R + R_s}{L} I - h(x, \dot{x}, I) - \frac{1}{L} V\right) + u_1 \dot{u}_1 \tag{43}$$

where $h(x, \dot{x}, I) = (k/L)(\dot{x}I/x^2)$. Since the controller consists of the outer and inner parts. For the outer part of the controller, that is, for $|s_2| \geq \varepsilon$, we have

$$\dot{V}_2 = s_2\left(\dot{I}_r + \frac{R + R_s}{L} I - h(x, \dot{x}, I) - \frac{\alpha}{L} |s_2|^{1/2} \operatorname{sgn}(s_2)\right) + \varphi_0 \tag{44}$$

where the function φ_0 can be written as

$$\begin{aligned}\varphi_0 &= -u_1 s_2/L + \beta u_1 |s_2|^{1/2} \operatorname{sgn}(s_2)\\ &= -\beta u_1 s_2\left(1 - \frac{1}{|s_2|^{1/2}}\right)\\ &= -\gamma \beta u_1 s_2\end{aligned} \tag{45}$$

with $0 \leqslant \gamma < 1$ and it is assumed that $\beta = 1/L$ for simplicity. Now the derivative of the Lyapunov function (45) satisfies the inequality

$$\dot{V}_2 \leqslant \left(\left| \dot{I}_r \right| + \frac{R + R_s}{L} I + |h(x, \dot{x}, I)| + \gamma\beta |u_1| - \frac{\alpha}{L} |s_2|^{1/2} \right) |s_2| = -\left(\frac{\alpha}{L} |s_2|^{1/2} - \mu \right) |s_2| \quad (46)$$

where $\mu = \left| \dot{I}_r \right| + I(R + R_s)/L + |h(x, \dot{x}, I)| + \gamma\beta |u_1|$. Since $|s_2| \geqslant \varepsilon$, if we choose $\alpha > L\mu/\sqrt{\varepsilon}$, then $\dot{V}_2 < 0$. Namely, whenever $|s_2| \geqslant \varepsilon$, $|s_2(t)|$ will strictly decrease until it reaches the set $|s_2| < \varepsilon$ in finite time and remains inside the set subsequently. For the inner part of the controller, that is, inside the set $|s_2| < \varepsilon$, the derivative of the Lyapunov function is

$$\dot{V}_2 = s_2 \left(\dot{I}_r + \frac{R + R_s}{L} I - h(x, \dot{x}, I) - \frac{\alpha}{L} |s_2|^{1/2} s_2 / \varepsilon \right) + \varphi_1 \quad (47)$$

with

$$\begin{aligned} \varphi_1 &= -u_1 s_2 / L + \beta u_1 |s_2|^{1/2} s_2 / \varepsilon \\ &= -\beta u_1 s_2 (1 - |s_2|^{1/2} / \varepsilon) \\ &= -\gamma_1 \beta u_1 s_2 \end{aligned} \quad (48)$$

where $0 < \gamma_1 < 1$, and again it is assumed that $\beta = 1/L$ for simplicity. Finally, we get

$$\begin{aligned} \dot{V}_2 &\leqslant \bar{\mu} |s_2| - \frac{\alpha}{\varepsilon L} |s_2|^{5/2} \\ &\leqslant -(1 - \theta) \frac{\alpha}{\varepsilon L} |s_2|^{5/2} \end{aligned} \quad (49)$$

with $0 < \theta < 1$ and $\bar{\mu} = \left| \dot{I}_r \right| + I(R + R_s)/L + |h(x, \dot{x}, I)| + \gamma_1 \beta |u_1|$. The inequality (49) is satisfied for all

$$|s_2| \geqslant \left(\frac{\varepsilon L \bar{\mu}}{\theta \alpha} \right)^{2/3} \quad (50)$$

Hence, the trajectory reaches the ultimate bound set $\Sigma = \{|s_2| < (\varepsilon\bar{\mu}/(\theta\alpha K_1))^{2/3} < \varepsilon\}$ in finite time. This means that the tracking error also stays around the origin, but not in the origin in general. Consequently the practical stability of the electrical system under the proposed SMC controller (41) is guaranteed for the given ultimate bound. It is clear that the stability condition is obtained as $\alpha > L\mu/\sqrt{\varepsilon}$. The stability analysis does not provide a straightforward condition for the control gain β because it is used for good tracking performance, and thus it can be selected arbitrarily to get a good steady-state response.

Robustness of the sliding mode current controller. From equation (40), the differential equation of the sliding surface including uncertainties can be written as

$$\dot{s}_2 = \dot{I}_r + \delta_0 I - \delta_1 V - h(x, \dot{x}, I) \quad (51)$$

where $h(\cdot)$ represents the nonlinear part of model (11), considered as a bounded disturbance, $|h(x, \dot{x}, I)| \leqslant \mu_0$, $\delta_0 = ((R + R_s)/L) + \Delta_0 > 0$, and $\delta_1 = (1/L) + \Delta_1 > 0$ with bounded inductance-related uncertainties Δ_0 and Δ_1. Using Lyapunov's stability theorem, one can found similar stability conditions as described above

$$\alpha > \frac{L\tilde{\mu}}{(1 + L\Delta_1)}, \varepsilon > |s_2| \geqslant \left(\frac{\varepsilon L \hat{\mu}}{\theta\alpha(1 + L\Delta_1)} \right)^{2/3} \quad (52)$$

where $\tilde{\mu} \geqslant \mu$ and $\hat{\mu} \geqslant \bar{\mu}$ due to the bounds of uncertainties and disturbance. Consequently, the practical stability of the system can be guaranteed under bounded uncertainties.

Experimental results

The experimental test results of the proposed cascade controllers for the magnetic levitation plant are provided in this section. The desired performance requirements are taken as (1) percentage overshoot $\leqslant 5\%$ and (2) maximum settling time $\leqslant 0.3$ s, for the position control. This means that the damping ratio should be $\varsigma_b = 0.69$ and the natural frequency is found as $w_{nb} = 19.3$ rad/s. The location of the third pole is selected as $p_0 = 40$. It is also assumed that the operating point of the system is $x_0 = 6$ mm which leads to $I_0 = 0.86$ A. Therefore, the control parameters based on the desired performance requirements and operating points are found from equation (22) as $k_{pb} = -199.7$, $k_{i2} = -633.2, k_{vb} = -2.82$ and $b_{sp} = 0.35$ for the PIV with the set point weighting controller. The derivative filter parameters are selected as $\varsigma_d = 0.9$ and $w_d = 471\,\text{rad}/s$.

For the PI current controller parameters, the desired performance requirements are taken as (1) percentage overshoot $\leqslant 1.5\%$ and (2) the peak time as $t_p = 0.015$ s. These lead to the damping ratio and natural frequency to be $\varsigma_e = 0.8$ and $w_{ne} = 350\,\text{rad}/s$, respectively. Hence the PI control gains are found from equation (15) as $k_{pe} = 50,000$ and $k_{ie} = 220$.

The integral SMC position control parameters are found as $\lambda = 60, \lambda_0 = 2000, I_m = 50$ and $\varepsilon = 0.03$. Finally, the SMC current control parameters are taken as $\alpha = 150$, $\beta = 50,000$ and $\varepsilon = 0.1$ in order to guarantee the stability condition $\alpha > L\mu/\sqrt{\varepsilon}$.

The experimental results are obtained for a pulse-like and sinusoidal position reference signals. Since the variations in the reference trajectories must be selected as a frequency below the -3 dB point of the electromagnet, first we find that the time constant of the coil is $\tau_e = 0.0375$s which results in a bandwidth of $1/\tau_e = 26.7\,\text{rad/s}$ or 4.25 Hz, and then the frequencies of the reference trajectories are taken as $f = 0.25$ Hz.

For a pulse-like reference signal with a 0.25-Hz frequency and a 2-mm peak-to-peak amplitude, the experimental test results are shown in Figures 5–8. While the operating point is taken as $x_0 = 6$ mm in control calculations, the reference trajectory varies from 8

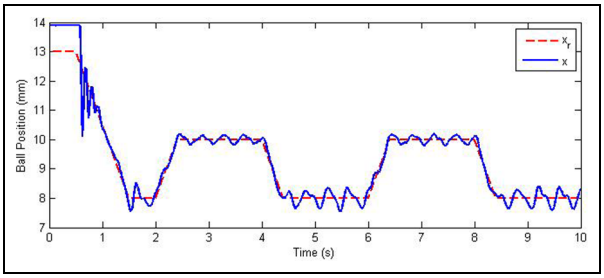

Figure 5. Position tracking performance of the PIV plus PI controller.

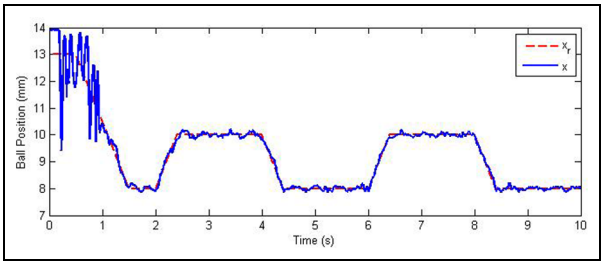

Figure 6. Position tracking performance of the SMC plus SMC controller.

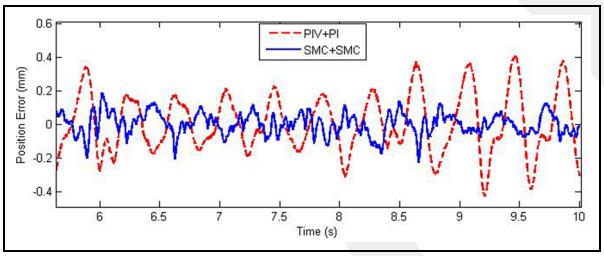

Figure 7. Position tracking error.

to 10 mm. Figure 5 shows the position tracking performance of the PIV plus PI controller, while Figure 6 shows the performance of the SMC plus SMC controller. It is seen that the SMC + SMC control approach gives better tracking performance than the PIV + PI controller since it holds the ball during startup and follows the reference position trajectory thereafter and has much smaller tracking error as seen in Figure 7. The small oscillations around the reference point are due to the effects of measurement error of the position sensor (see its sensitivity in Table 1), sampling and measurement noise. It is seen from Figure 7 that the position error is limited to about ± 0.4 mm for the PIV + PI controller, but on the other hand, the tracking error approaches to ± 0.1 mm with increasing operation time for the SMC + SMC controller. Figure 8 shows the response of the coil current of cascade controllers. The SMC + SMC controller has a fast variation in the applied current, which is necessary to eliminate the effects of inductance uncertainty and to provide a highly satisfactory tracking performance.

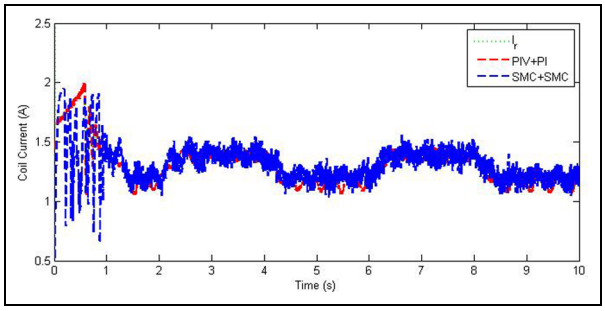

Figure 8. Applied coil current for the maglev system.

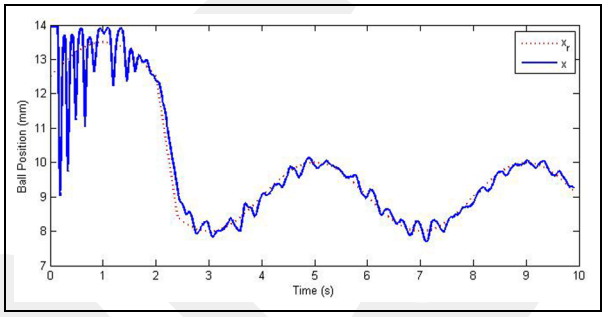

Figure 9. Sinusoidal tracking performance of the SMC plus SMC controller.

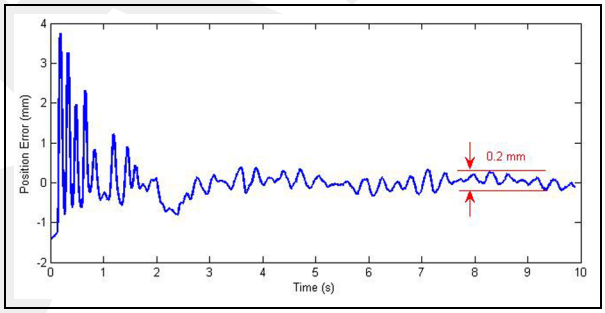

Figure 10. Sinusoidal tracking error.

In the second trial, tracking of a 0.25-Hz sinusoidal reference signal with a 2-mm peak-to-peak amplitude, $x_r = 9 + \sin(1.57t)$, is evaluated. The performance of the system under the proposed cascade SMC control law is illustrated in Figures 9–13. The corresponding position tracking response is given in Figure 9 where it is clear that the controller holds the ball during startup and follows the reference position trajectory thereafter. The reference tracking error, seen in Figure 10, oscillates between ± 0.1 mm at steady-state for the sinusoidal reference signal. The applied voltage shown in Figure 11 varies around 14 V. The applied current and the current tracking error are displayed in Figures 12 and 13, respectively. It is clear that the current error reaches 0 in a short time and stays around 0 thereafter.

It should be noted that it is not possible to provide a healthy comparison with the literature since the

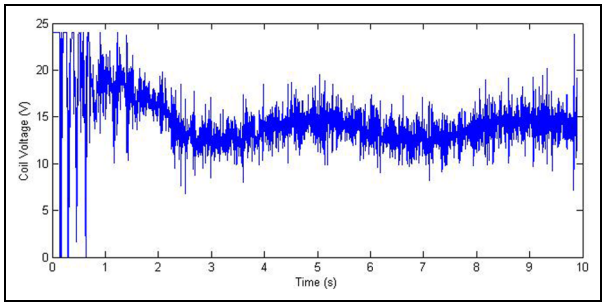

Figure 11. Applied coil voltage.

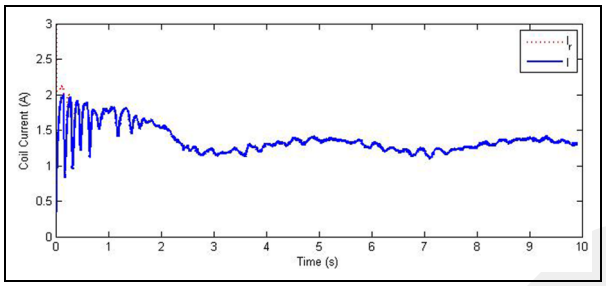

Figure 12. Applied coil current.

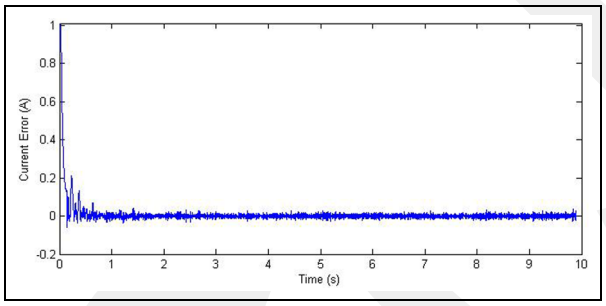

Figure 13. Current tracking error.

experimental setup is different from the ones used in the literature. On the other hand, it was reported that the tracking error oscillates between ±0.4 mm with linear controllers and ±0.1 mm with some nonlinear controllers.[7] Therefore, while our experimental setup is different, the SMC-based cascade controller presented here provides the best possible results with ±0.1 mm tracking error for the single-axis magnetic levitation plant.

Conclusion

An integral SMC plus output feedback SMC-based and a PIV plus PI cascade controllers are designed for tracking control of a magnetic levitation plant. The proposed cascaded SMC controllers are able to stabilize the magnetic levitation system from tough startup conditions to the desired operating points. To deal with the unstable nature and uncertain nonlinear dynamics of the plant, the magnetic levitation plant is represented with electrical and mechanical models, and the control problems of these parts are treated with sliding mode cascade controllers. The experimental results show that the proposed control method provides a highly satisfactory tracking control performance in the presence of inductance originated disturbance and uncertainties. The cascaded SMC controllers keep the current error around 0 and provide a position error around ±0.1 mm at the steady-state, which is very small compared to the literature. This work also shows that it is possible to use sliding mode controllers in cascade control form for getting good performances in the electromechanical systems.

Declaration of conflicting interests

The author(s) declared no potential conflicts of interest with respect to the research, authorship and/or publication of this article.

Funding

This work was supported by Turkish Scientific and Research Council (TUBITAK) under project number 113E329.

References

1. Berdy DF, Valentino DJ and Peroulis D. Kinetic energy harvesting from human walking and running using a magnetic levitation energy harvester. *Sensor Actuat A: Phys* 2015; 222: 262–271.
2. Jungmayr G, Marth E, Panholzer M, et al. Design of a highly reliable fan with magnetic bearings. *Proc IMechE, Part I: J Systems and Control Engineering* 2016; 230: 361–369.
3. Ozturk K, Sahin E, Abdioglu M, et al. Comparative study of the magnetic stiffness, levitation and guidance force properties of single and multi seeded YBCOs for different HTS–PMG arrangements. *J Alloy Compd* 2015; 643: 201–206.
4. Hasirci U, Balikci A, Zabar Z, et al. A novel magnetic-levitation system: design, implementation, and nonlinear control. *IEEE T Plasma Sci* 2011; 39: 492–497.
5. Luguang Y. Progress of the maglev transportation in China. *IEEE T Appl Supercon* 2006; 16: 1138–1141.
6. El Hajjaji A and Ouladsine M. Modeling and nonlinear control of magnetic levitation systems. *IEEE T Ind Electron* 2001; 48: 831–838.
7. Barie W and Chiasson J. Linear and nonlinear state-space controllers for magnetic levitation. *Int J Syst Sci* 1996; 27: 1153–1163.
8. Yamamura S and Yamaguchi H. Electromagnetic levitation system by means of salient-pole type magnets coupled with laminated slotless rails. *IEEE T Veh Technol* 1990; 39: 83–87.
9. Cho D, Kato Y and Spilman D. Sliding mode and classical controllers in magnetic levitation systems. *IEEE Control Syst* 1993; 13: 42–48.
10. Beltran-Carbajal F, Valderrabano-Gonzalez A, Rosas-Caro JC, et al. Output feedback control of a mechanical

system using magnetic levitation. *ISA T* 2015; 57: 352–359.
11. Morales R and Sira-Ramírez H. Trajectory tracking for the magnetic ball levitation system via exact feedforward linearisation and GPI control. *Int J Control* 2010; 83: 1155–1166.
12. Nielsen C, Fulford C and Maggiore M. Path following using transverse feedback linearization: application to a maglev positioning system. In: *Proceedings of the American control conference, 2009 (ACC '09)*, St. Louis, MO, 10–12 June 2009, pp.3045–3050. New York: IEEE.
13. Zhang J, Tao T, Mei X, et al. Non-linear robust control of a voltage-controlled magnetic levitation system with a feedback linearization approach. *Proc IMechE, Part I: J Systems and Control Engineering* 2011; 225: 85–98.
14. El Rifai OM and Youcef-Toumi K. Achievable performance and design trade-offs in magnetic levitation control. In: *Proceedings of the 1998 5th international workshop on advanced motion control, 1998 (AMC '98-Coimbra)*, Coimbra, 29 June–1 July 1998, pp.586–591. New York: IEEE.
15. Kim YC and Kim K-H. Gain scheduled control of magnetic suspension system. In: *Proceedings of the American control conference 1994*, Baltimore, MD, 29 June–1 July 1994, vol. 3, pp.3127–3131. New York: IEEE.
16. Baranowski J and Piątek P. Observer-based feedback for the magnetic levitation system. *T I Meas Control* 2012; 34: 422–435.
17. Al-Araji AS. Cognitive non-linear controller design for magnetic levitation system. *T I Meas Control*. Epub ahead of print 27 April 2015. DOI: 10.1177/0142331215581639.
18. Benitez-Pérez H, Ortega-Arjona J, Cardenas-Flores F, et al. Reconfiguration control strategy using Takagi–Sugeno model predictive control for network control systems—a magnetic levitation case study. *Proc IMechE, Part I: J Systems and Control Engineering* 2010; 224: 1022–1032.
19. Chen S-Y, Lin F-J and Shyu K-K. Direct decentralized neural control for nonlinear MIMO magnetic levitation system. *Neurocomputing* 2009; 72: 3220–3230.
20. Al-Muthairi NF and Zribi M. Sliding mode control of a magnetic levitation system. *Math Probl Eng* 2004; 2004: 93–107.
21. Lin F-J, Chen S-Y and Shyu K-K. Robust dynamic sliding-mode control using adaptive RENN for magnetic levitation system. *IEEE T Neural Networ* 2009; 20: 938–951.
22. Lin F-J, Teng L-T and Shieh P-H. Intelligent adaptive backstepping control system for magnetic levitation apparatus. *IEEE T Magn* 2007; 43: 2009–2018.
23. Bächle T, Hentzelt S and Graichen K. Nonlinear model predictive control of a magnetic levitation system. *Control Eng Pract* 2013; 21: 1250–1258.
24. Iplikci S and Bahtiyar B. A field-programmable gate array implementation of a real-time nonlinear Runge–Kutta model predictive control. *T I Meas Control* 2016; 38: 555–564.
25. Javadi A and Pezeshki S. A new model-free adaptive controller versus non-linear H_∞ controller for levitation of an electromagnetic system. *T I Meas Control* 2013; 35: 321–329.
26. Kumar EV and Jerome J. LQR based optimal tuning of PID controller for trajectory tracking of magnetic levitation system. *Procedia Eng* 2013; 64: 254–264.
27. Jayawant BV and Rea DP. New electromagnetic suspension and its stabilisation. *P I Electr Eng* 1968; 115: 549–554.
28. Shtessel Y, Edwards C, Fridman L, et al. *Sliding mode control and observation*. New York: Springer, 2013.
29. Ablay G. Variable structure controllers for unstable processes. *J Process Contr* 2015; 32: 10–15.